Journal of Fluorine Chemistry 243 (2021) 109738

Contents lists available at ScienceDirect

Journal of Fluorine Chemistry

journal homepage: www.elsevier.com/locate/fluor

Microstructural characterization of grade 300 and grade 350 maraging steels and electrochemical study in hydrofluoric solution

Mauro Andrés Cerra Florez [a,b,*], Úrsula Cid Pereira [a], Jorge Luiz Cardoso [a], Francisco José dos Santos Oliveira [a], Walney Silva Araújo [a], Gemma Fargas Ribas [b], Hamilton Ferreira Gomes de Abreu [a], Marcelo José Gomes da Silva [a]

[a] Department of Metallurgical and Materials Engineering, Federal University of Ceará, Campus do Pici, bloco 729, Fortaleza, 60440-900, Ceará, Brazil
[b] CIEFMA-Dept. of Materials Science and Engineering, Universitat Politècnica de Catalunya, EEBE-Campus Diagonal Besòs, 08019, Barcelona, Spain

ARTICLE INFO

Keywords:
Aqueous corrosion
Heat treatments
Hydrofluoric acid
Maraging steels
Raman analysis

ABSTRACT

The electrochemical behavior of solution-annealed grade 300 and grade 350 maraging steels subjected to two different aging temperatures in an aqueous hydrofluoric acid (HF) medium was evaluated. The microstructural and hardness studies showed the effects of the chemical composition and heat treatments on the material properties. Although it is not possible to observe them, the fine intermetallic composites deposited during aging allow a significant increase in the hardness of materials, which was reduced when aged at 560 °C, where there was formation of reverted austenite. The results showed that, in both steels, solution-annealed samples that were not aged showed a better corrosion behavior than the aged samples. The reversion of austenite during aging at temperatures above 560 °C increases the phase limits and its susceptibility to corrosion. The greater amount of cobalt and titanium in grade 350 maraging steel increases the amount of fine intermetallic precipitate rich in molybdenum and titanium during aging, therefore improving its mechanical properties, but also reducing its corrosion resistance.

1. Introduction

Maraging steels contain 18 % nickel and low carbon content, as well as cobalt (7–12 %), molybdenum (3–5 %), and titanium (0.2–1.6 %) in their composition. Known for their ultra-high strength and superior toughness and malleability [1,2], maraging steels are so named for their microstructure comprising α'-martensite (Mar) and precipitated intermetallic compounds formed due to aging heat treatments (Aging), which strongly increases their mechanical strength [1–3]. Alloy elements such as cobalt increase the transformation temperature of martensite. In concentrations between 6 and 11 %, the solubility of molybdenum in martensite decreases, allowing the precipitation of intermetallic compounds during the aging process, therefore increasing yield stress [2–4]. At temperatures in the range of 420−570 °C, molybdenum and titanium form precipitations of Ni_3(Ti, Mo) and Fe_2(Ti, Mo) in the grain boundaries and in the martensite dislocations [4–6].

These steels are used in the manufacture of centrifuge rotors to enrich uranium for the production of nuclear fuel. In these applications, maraging components are exposed to atmospheres rich in fluorine and fluoride acid residues that are highly corrosive [7–9]. Bradhurst and Heuer [9] investigated the susceptibility of grade 350 maraging steel to crack propagation by performing tensile tests in closed chambers containing an atmosphere rich in uranium hexafluoride (UF_6) and/or hydrofluoric acid (HF) at 70 °C. The results showed that when the UF_6 was dry, the steel showed good resistance to cracking. However, in conditions in which hydrofluoric acid cracks appeared, the failure stress decreased. They concluded that this hydrogen embrittlement failure mechanism is linked to the hydrogen produced in reactions with the metal. It is also mentioned in the literature that fluorine may react, forming metallic fluorides that would be protective, and even the use of anodizers to improve the corrosion resistance was suggested [8], but no test showed any result that confirms this information.

Poormina et al. [10] studied in two works grade 250 maraging steels solution annealed at 815 °C for 1 h and aged (without information on aging conditions) using polarization tests and electrochemical impedance spectroscopy in various concentrations of phosphoric acid solution. They concluded that the increase in the acid concentration decreases the corrosion resistance of this steel, showing a higher corrosion rate. They

* Corresponding author at: Federal University of Ceará, Zip Code 60440-900, Brazil.
E-mail address: mauro.cerra@gmail.com (M.A. Cerra Florez).

https://doi.org/10.1016/j.jfluchem.2021.109738
Received 6 November 2020; Received in revised form 18 January 2021; Accepted 22 January 2021
Available online 27 January 2021

also mentioned that the solution-annealed steel showed better corrosion behavior than the aged one because of the presence of intermetallic precipitates (with different matrix composition), causing deformation fields to form around these precipitates (due to the incompatibility of the network between the precipitate and the matrix) and deterioration of the steel, leading to the corrosion of aged samples when compared with the solution-annealed ones.

Sanatkumar et al. [11] and Kumar [12] studied welded grade 250 maraging steel in different concentrations of hydrochloric acid (HCl) solutions. They used the polarization and electrochemical impedance techniques and found that as the acid concentration increases, the aged steel has less corrosion resistance and the corrosion rate increases, but the corrosion potential shifts to less negative values. They observed the surface of the samples using SEM after the corrosion tests and found that the surface was deteriorated, with signs of intergranular corrosion.

This work aims to characterize both maraging steel grades, 300 and 350, and to study the electrochemical behavior in hydrofluoric acid solution. It also aims to understand the influence of chemical composition and heat treatments such as solution annealing and aging on their corrosion resistance.

2. Materials and methods

2.1. Materials

The materials used in this research were grade 300 and 350 maraging steels, and their chemical compositions are shown in Table 1.

2.2. Heat treatments

The samples were cut to 20 mm x 10 mm x 5 mm. Considering the chemical composition, a thermodynamic simulation was performed using the Thermo-Calc® software (TCFE6 database), which allowed to obtain mass fraction diagrams of the phases found in the steel through thermodynamic equilibrium calculations in order to obtain phase diagrams. The solution annealing temperature (840 °C) and the aging temperatures (480 °C and 560 °C) were selected according to the thermodynamic simulations and the information found in the literature [2,3,5,6]. The time chosen for the solution annealing and aging heat treatments were 1 h and 3 h, respectively. The heat treatments were carried out in a muffle furnace and air-cooled.

2.3. Materials characterization

In order to identify the phases, X-Ray Diffraction Analysis was carried out using a Panalytical X'Pert Pro diffractometer with CoKα radiation (0.1789 nm). The 2θ angle ranged from 40° to 110°, with an angular step of 0.02° per scan and 3 s of counting time. The voltage and current used were 40 kV and 45 mA, respectively. The identification of the phases was carried out with the X'PertHighScore Plus® software from Panalytical®. The phase quantification through X-ray diffraction (XRD) was carried out using the direct comparison method as described by Pardal et al. [13] and Santos et al. [14], assuming that the chemical composition of the austenite and martensite phases may be different. Three peaks of martensite {111}, {200}, {211}, and three peaks of austenite {111}, {200}, {220}, were analyzed, and in order to minimize the effect of the texture, the average values of all diffraction peaks were calculated and compared [14]. Microstructural analysis with EBSD was performed, processed, and plotted on the Oxford/HKL Channel 5 software to confirm the phases on the steels in each condition.

Following the heat treatment, the samples were ground using SiC paper up to 2000 mesh with continuous water flow, then polished with 1 μ and 0.05 μ alumina (Al_2O_3), rinsed with distilled water and alcohol, and blow-dried. Two etching steps were used to reveal the microstructure: electrolytic etching with chromic acid H_2CrO_4 (20 %) solution for 15 s at 10 V and then etching with Nital 2% for 10 s in order to reveal the prior austenite grain boundaries. A Zeiss® model AX10 optical microscope was used to observe the microstructure and the ImageJ software was used to calculate the prior austenite grain size through the method described by Silva et al. [15] based on ASTM E112-96 [16]. To reveal the martensite microstructure, an electrolytic etching (10 V) was used in a chromic acid H_2CrO_4 (20 %) solution for 15 s, and then etched with Marble solution (4 g $CuSO_4$ + 20 mL HCl + 20 mL H_2O) for 10 s. After that, the samples were observed in the Scanning Electron Microscope (SEM) model quanta 450.

Rockwell C hardness tests (HRc) were performed according to ASTM E18 (2003) standard using a Microtest model 737 durometer with a conical diamond penetrator. The preload and main load applied were 10 and 150 kgF, respectively. The highest and lowest values were eliminated, and the average was taken from the remaining values.

2.4. Electrochemical measurements

Electrochemical measurements were carried out on a Metrohm® Autolab PGSTAT 302 N potentiostat/galvanostat controlled by the NOVA® software for data acquisition. Open Circuit Potential (OCP), Linear Polarization, and Electrochemical Impedance Spectroscopy tests were performed. A conventional three-electrode cell was used. An Ag/AgCl (saturated KCl) electrode was used as reference, a platinum plate with a geometric area of approximately 130 mm^2 was used as counter electrode, and the working electrodes were the samples of both maraging steels. Samples were ground up to 2000 mesh, rinsed with distilled water and ethanol to degrease them and then blow-dried. Before the tests, an exposed area of approximately 30 mm^2 was fixed on the samples. The measurements were taken in a Faraday cage at room temperature. The OCP tests were performed by submerging the samples in 0.01 M HF (hydrofluoric acid) solution for 30 min. The linear polarization curves were obtained in a potential range from -200 to +600 mV around the OCP with a scan rate of 1 mV/s in accordance with the literature [10–12]. The tests ended when the current density reached 1 mA. The Electrochemical Impedance Spectroscopy tests were performed after potential stabilization for 30 min. The sinusoidal disturbance of the corrosion potential was 10 mV, the frequency range used was from 50 kHz to 0.01 Hz, and the reading rate was 10 points per decade of frequency.

After the polarization tests, the surface of the samples was observed in the SEM Phenom XL with EDS detector. Raman spectroscopy analysis was also performed in a Renishaw inVia ™ confocal Raman microscope with a Neon Laser (λ ~ 532 nm), while the analysis of Raman intensities was performed using the WIRE software.

3. Results and discussion

3.1. Thermodynamic analysis

The chemical composition of the steels allowed the performance of a thermodynamic simulation in the Thermo-Calc® software, where mass fraction diagrams were generated to show the quantities of the phases

Table 1
Chemical compostions (% wt) of the grade 300 and 350 maraging steels.

Elements:	Fe	Ni	Co	Mo	Ti	Cr	V	Si	Al	Cu	Mn	C
Mar300	Bal.	18.28	9.51	4.80	0.73	0.12	0.10	0.08	0.07	0.05	0.03	<0.01
Mar350	Bal.	17.65	11.65	4.69	1.44	0.05	0.10	0.04	0.06	0.01	0.02	0.002

found in the steels according to the temperature. The mass fraction diagram for grade 300 maraging steel is shown in Fig. 1. This result made it possible to identify areas of stability for the predicted phases. At temperatures between 670 °C and 1380 °C, austenite (FCC) is the only phase present in this steel. At higher temperatures, the liquid is produced, and at lower temperatures, martensite (BCC) is formed and the Mu and Ni_3Ti phases are segregated. As the temperature decreases, the amount of martensite increases proportionally to the austenite decrease. The segregated phases reach a maximum amount which remains fixed until reaching room temperature, with the particularity that the Mu phase is slightly larger than the titanium nitrite phase.

Fig. 2 shows the mass fraction diagram for grade 350 maraging steel. The same phases found in the grade 300 maraging steel diagram were identified, and it is possible to find minor differences. One of these differences is that the austenite stability area (FCC) is slightly smaller, and the temperatures at which this phase is the only phase present are in the range of 690−1340 °C (solution annealing). The temperatures at which martensite (BCC), Mu, and Ni_3Ti are formed are slightly higher. The number of segregates is relatively equal at temperatures below 450 °C.

3.2. Characterization of the samples

Fig. 3 shows the diffractograms of grade 300 and grade 350 maraging steels solution annealed at 840 °C for 1 h. Only peaks of body-centered cubic (BCC) α' phase are found [15]. This transformation occurs because of the high nickel content, the low carbon content and the shear phenomenon, and it is a structural modification that occurs with any cooling rate. The martensite formed is softer and more resistant than the tetragonal one (BCT) [14,17,18]. Fig. 4 shows the maraging steels in the solution annealed condition, where the prior austenite grain boundaries for both grades, 300 (Fig. 4(a)) and 350 (Fig. 4(b)), can be observed. The average grain size is 24.6 μm and 108.69 μm, respectively. Fig. 5 shows the SEM images of the maraging steels, grades 300 (Fig. 5(a)) and 350 (Fig. 5(b)). The microstructure of this material comprises well-defined martensite laths and is similar in all heat treated conditions.

Fig. 6 shows the diffractogram of grade 300 and grade 350 maraging steels solution annealed at 840 °C for 1 h and aged at 480 °C for 3 h. It can be observed that the existing peaks are the same as in the solution annealed condition and correspond to 100 % of the α' martensite phase (CCC), which is characteristic of this material, with orientation {111}, {200} and {211} [15]. It is also worth mentioning that the intermetallic precipitates produced during aging were not found in the diffractograms. According to Santos [14] and Lima Filho [17], this is due to the technique limitations to detect fractions below 5% in volume. Fig. 7 shows the grains of maraging steel grades, 300 (Fig. 7(a)) and 350 (Fig. 7(b)), both solution annealed at 840 °C for 1 h and aged at 480 °C for 3 h,

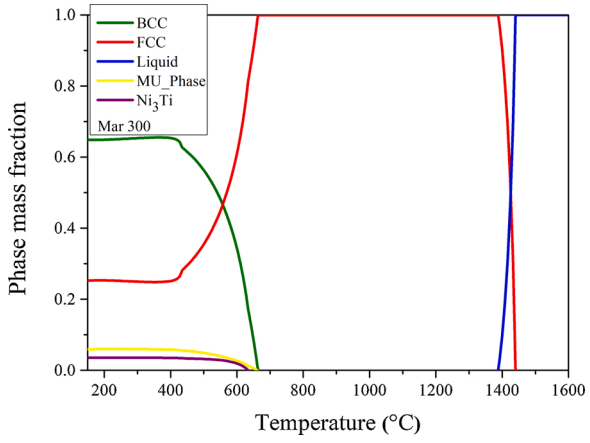

Fig. 1. Mass fraction diagram of grade 300 maraging steel.

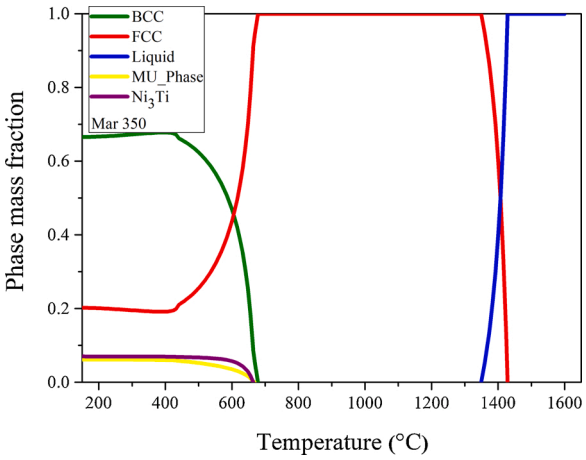

Fig. 2. Mass fraction diagram of grade 350 maraging steel.

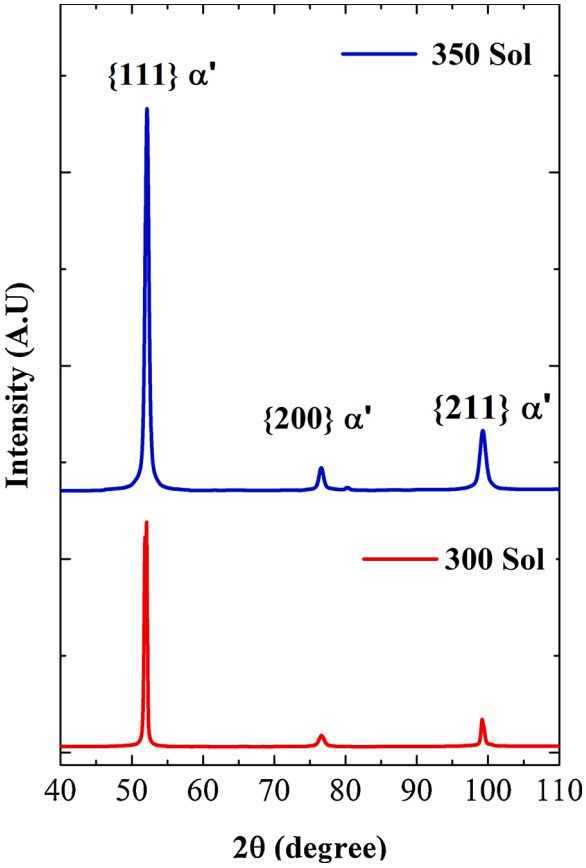

Fig. 3. X-ray diffraction pattern of the grade 300 and 350 maraging steel samples solution treated at 840 °C, showing the peaks of martensite.

while the microstructure for both steels are shown in Fig. 8. The average grain size is 28.6 μm and 103.4 μm, respectively. In the microstructure, it was possible to observe the martensite laths along the characteristic grains.

Fig. 9 shows the diffractogram of grade 300 and grade 350 maraging steels solution annealed at 840 °C for 1 h and aged at 560 °C for 3 h. It can be observed that the existing peaks are the same as in the previous conditions and correspond to the α' martensite phase (CCC), which is characteristic of this material, with orientation {111}, {200} and {211} [15], but peaks were also found corresponding to the austenite phase (FCC) in both steels, with orientation {111}, {200} and {220} [19]. The

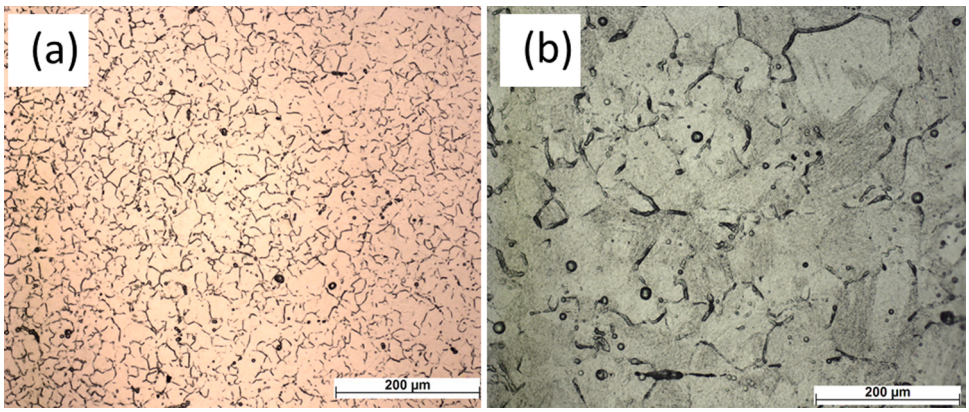

Fig. 4. Optical microscopy images of maraging steels (a) 300 and (b) 350 in the solution annealed condition.

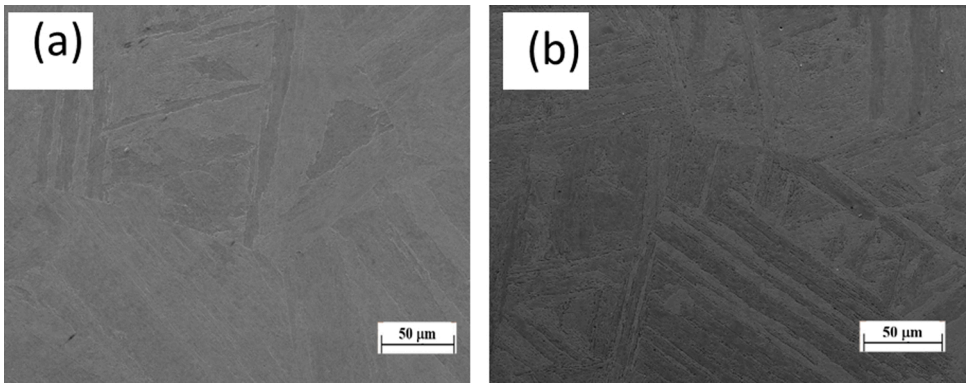

Fig. 5. SEM of the microstructure of maraging steels (a) 300 and (b) 350 in the solution annealed condition.

volume fraction of reverted austenite was determined using the direct comparison method described in the literature [13,14], with 13 vol.% on grade 350 maraging steel and 8 vol.% on grade 300 maraging steel, approximately. The austenite precipitation during aging is attributed to the nickel and molybdenum contents in both martensite and intermetallic compounds. Austenite precipitates in the contours of the martensite slats, absorbing these elements from the dissolution of the martensite into intermetallic compounds rich in Ni, Ti and Mo [14,15]. To complement the previous result, Fig. 10 shows SEM/EBSD images taken from the sample of grade 300 maraging steel aged at 560 °C for 3 h. In Fig. 10 (a), a general area is shown where thin slats with high relief corresponding to another phase are observed. Fig. 10 (b) shows the area where the EBSD analysis was performed and where the previously mentioned slats are also seen, and in Fig. 10(c) it is possible to see the EBSD phase map showing the BCC martensitic matrix that confirms reverted austenite (slat-shaped austenite) as described by [20]. Fig. 10 (d) shows the color key for the phases. Likewise, no intermetallic compounds were detected by XRD and EBSD in this condition.

Fig. 11 shows the grains of both grade 300 (Fig. 11(a)) and grade 350 (Fig. 11(b)) maraging steels. The average grain size is 28.1 µm and 107.2 µm, respectively. Fig. 12 shows the SEM images of grade 300 (Fig. 12(a)) and grade 350 (Fig. 12(b)) maraging steels. As before, martensite laths can be observed.

Table 2 shows the hardness measurements and the grain size for each heat treatment carried out in both maraging steels grades, 300 and 350. According to the results, steels in the solution annealing condition have an average hardness lower than in the aged condition, and among them grade 350 maraging steel showed slightly higher values when compared with grade 300 maraging steel. This difference could be explained by the chemical composition of the steels, according to Lima Filho [17], who analyzed the solution treatment at various temperatures, indicating that at temperatures above 1000 °C, Ni_3Ti precipitation could occur in grade 300 maraging steels. With a temperature of 840 °C, the considerable increase of titanium content in grade 350 maraging steel (twice as much as grade 300 maraging steel) could have caused the formation of this compound at the temperature used in this work. This can be confirmed by the thermodynamic diagrams in Figs. 1 and 2. They clearly show that the temperature for the formation of Ni_3Ti increases and the amount of Ni_3Ti formed in grade 350 maraging steel is higher when compared with the diagram for grade 300 maraging steel.

The analysis of the aging conditions shows that grade 350 maraging steel had greater hardness than grade 300 maraging steel because of the higher amount of cobalt and titanium found in the former. The effect of cobalt on the precipitation of intermetallic compounds formed by molybdenum, nickel, and titanium during aging is well known [1,21]. It is understandable that a greater amount of cobalt and titanium in grade 350 maraging steel increases the amount of precipitates, leading to a greater hardness in the material when compared with grade 300 maraging steel.

When comparing the values obtained from the two types of aging, aging at 560 °C for 3 h resulted in an average hardness lower than the in the aging at 480 °C for 3 h. This can be explained by the formation of reverted austenite. The precipitation of this phase during the aging of maraging steel leads to a decrease in their mechanical properties [1,5,14,15]. This is because of the dissolution of intermetallic compounds rich in nickel and molybdenum and the transformation of martensite into austenite, and the decrease in these phases impairs the mechanical properties [5,15,21]. In all conditions studied, the grains of the grade 350 maraging steel were bigger than the grains of grade 300 maraging steel, which can be an effect of the composition or manufacture process of these steels.

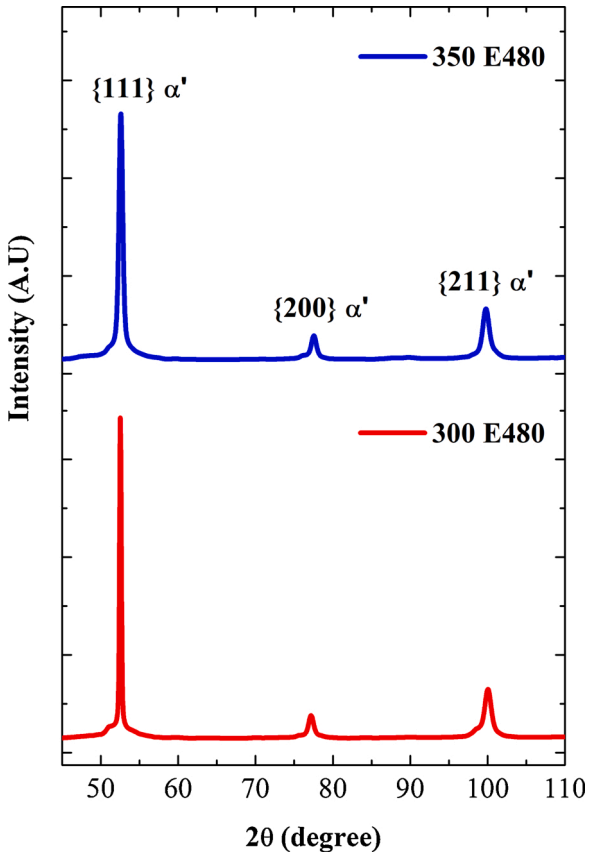

Fig. 6. X-ray diffraction pattern of the grade 300 and 350 maraging steel solution treated at 840 °C for 1 h and aged at 480 °C for 3 h, showing the peaks of the martensite.

3.3. Electrochemical measurements

The curves for the OCP, linear polarization, and EIS are shown in Figs. 13–15, respectively. The OCP values were taken with the sample in equilibrium with the solution. The corrosion current density values were obtained using the Tafel curves, while the corrosion resistance value was estimated considering the initial value of the arc along with the resistance value of the solution by extrapolating the arc to the point where it would cut the Z real axis.

Fig. 13 shows the OCP curves of maraging steels in hydrofluoric acid solution for all conditions studied. The quantitative results for the OCP measurements are shown in Table 3. Changes in the potential and direction of each curve show that the reactions are taking place on the surface, which indicates their electrochemical nature [22]. The solution treated samples (300 Sol and 350 Sol) in general showed a more noble behavior than the aged samples, in accordance with [10,22–24], and the curve of grade 350 maraging steel showed more noble potentials than grade 300 maraging steel. This can be associated with the greater amount of alloying elements such as cobalt and titanium in grade 350 maraging steel. It can also be observed that between the two aging conditions, samples treated at 480 °C (300 E480 and 350 E480) showed a more noble behavior than those treated at 560 °C (300 E560 and 350 E560), which can be attributed to the fact that no austenite was formed in the first condition. Finally, it should be noted that according to the curves and the E_{ocp}, in the two aging conditions studied, grade 300 maraging steel showed a relatively more noble behavior than grade 350 maraging steel. This can be associated with the greater amount of precipitated intermetallic compounds in grade 350 maraging steel when compared with the aged grade 300 maraging steel.

Fig. 14 shows the linear potentiodynamic polarization curves for both maraging steel grades under study and Table 3 shows the corrosion potential (V_{corr}) and corrosion current density (I_{corr}). The analysis of these curves shows that none of the maraging steel grades had passivation in the anodic branch as reported by Poormina [10], Sanatkumar [11], El-Mahdy [22] and Madhusudhan [24], who studied the behavior of these steels in acid solutions. The same behavior found in OCP curves can also be found in the linear potentiodynamic polarization curves. The solution annealed samples showed better performance than the aged ones. Among the aged samples, samples 300 E480 and 350 E480 showed better performance than samples 300 E560 and 350 E560, and in all aging conditions, grade 300 maraging steel showed better results than grade 350 maraging steel.

The solution treated sample of grade 350 maraging steel had a more noble corrosion potential (V_{corr}) than the other samples. The I_{corr} for the other samples were about the same, but the corrosion potential varied. Thus, the most noble behavior was found for the sample 300 Sol, followed by 300 E480, 350 E480, 300 E560, and finally 350 E560, similarly as the OCP results. The behavior in the cathode branch of all curves is similar. According to El-Mahdy [22], the evolution of hydrogen reduction reaction on the steel surface is under activation control, while the anodic branch suggests dissolution of the material. The absence of film formation can be explained by observing the studies [10,11,22,24], where the samples were immersed in solutions with phosphoric acid and hydrochloric acid. These studies mention the reactivity of the phosphorus ions and mainly the chlorine ion as the causes for the breakdown of the formed protective film, allowing the solution to continue dissolving the material. In this study, it is possible to associate the same behavior due to the well-known reactivity of the fluoride ion.

The impedance curves in Fig. 15 and Table 3 show the corrosion resistance values, confirming the same behavior pattern found in both OCP and polarization curves. They show that the solution annealed

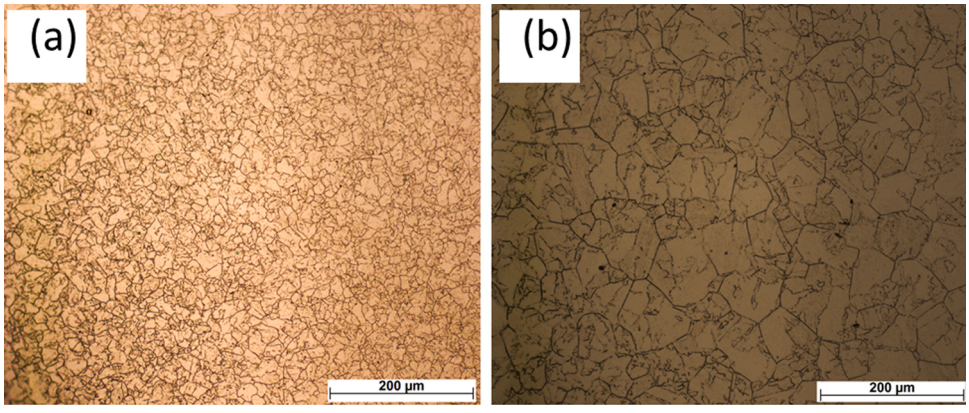

Fig. 7. Optical microscopy images of maraging steels (a) 300 and (b) 350 in the solution annealed condition at 840 °C for 1 h and aged at 480 °C for 3 h.

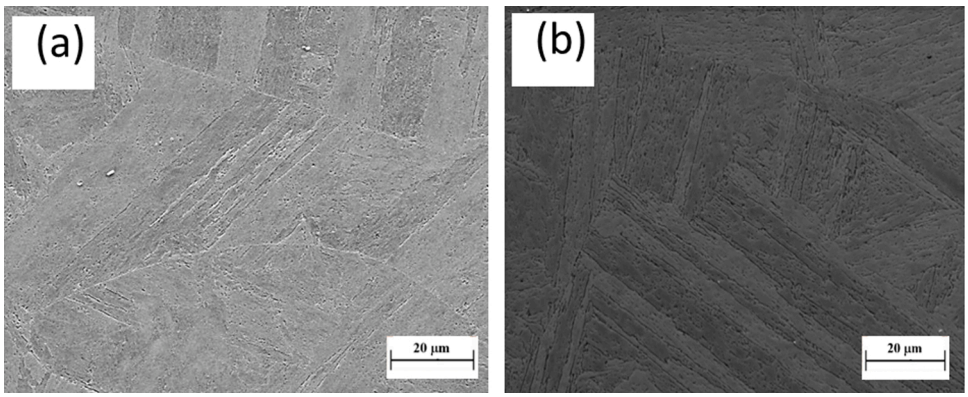

Fig. 8. SEM of the microstructure of maraging steels (a) 300 and (b) 350 solution annealed at 840 °C for 1 h and aged at 480 °C for 3 h.

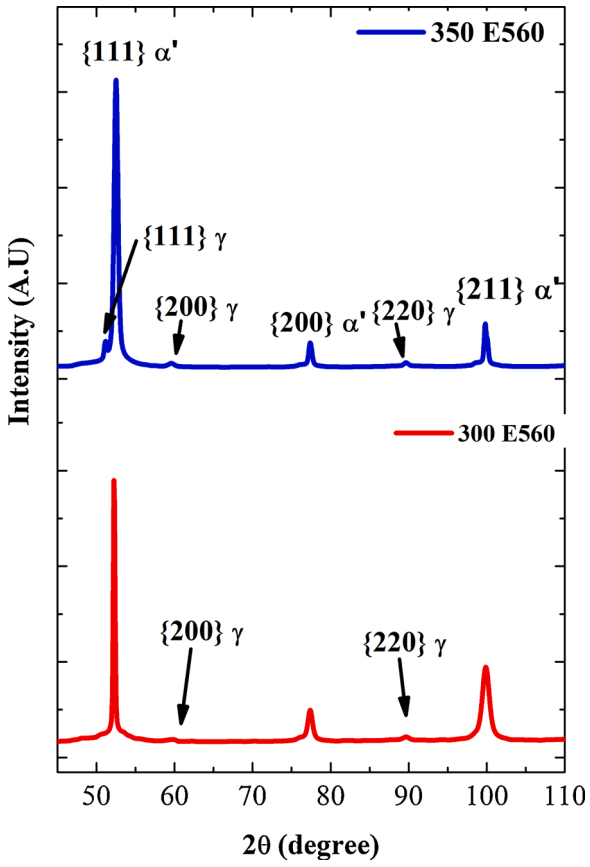

Fig. 9. X-ray diffraction pattern of the grade 300 and 350 maraging steel solution treated at 840 °C for 1 h and aged at 560 °C for 3 h, showing the peaks of the austenite.

samples had a larger capacitive loop than the aged ones, and among these samples, those treated at 480 °C had a larger loop than those treated at 560 °C. It is also possible to state that the semicircular shape of the arcs shows that corrosion is controlled by the charge transfer process between the solution and the metal surface [11,23]. It is important to highlight how the effect of the chemical composition and the intermetallic precipitates formed during the aging cause a decrease in the corrosion resistance of the material. This occurs due to differences in composition between the formed phases, with a more noble behavior in the solution annealed condition, and between the two steels, with grade 350 maraging steel showing better corrosion resistance because of its greater amount of alloying elements such as titanium and cobalt. In the aging condition, grade 300 maraging steel showed better behavior, and the samples treated at 560 °C had the lowest capacitive arc due to the influence not only of intermetallic compounds but also of the reversion of austenite in their microstructure.

The behavior of each steel can be explained according to the corrosion potential, current density, capacitive arc, as well as the chemical composition and the microstructure of the material. With solution annealed maraging steels, their behavior may have been influenced by the distribution of the alloy elements and uniformity of the martensitic phase, and the good performance of grade 350 maraging steel is mainly due to the higher content of cobalt and titanium. The poor performance of aged steels is due to the precipitation of intermetallic compounds during the aging heat treatment. This precipitation leads to the depletion from the metallic matrix of elements such as nickel, molybdenum and titanium, which are known for their good corrosion resistance. As a result, small galvanic piles are formed, reducing the corrosion resistance of the material [10,11,22].

With samples aged at 480 °C, small deformed loops were formed linking the capacitance distribution with the inhomogeneity on the electrode surface [11]. Grade 300 maraging steel had a higher capacitive arc than grade 350 maraging steel, which can be explained by the chemical composition of the steels. The steel with higher cobalt and titanium content could be expected to have better corrosion resistance. However, as mentioned earlier, during aging, the higher cobalt content leads to a greater precipitation of the intermetallic compounds, while the higher titanium content causes the formation of more precipitates, thus improving the mechanical properties but also decreasing the corrosion resistance by increasing galvanic pairs between the intermetallic phases and the steel matrix. This same relationship applies to the steels aged at 560 °C.

The poorer corrosion resistance of the steels aged at 560 °C results from precipitation of austenite inside the material, as mentioned before. The reverted austenite is rich in nickel and molybdenum, forming a new focus of galvanic pair within the metal together with the increase in the interphase between austenite and martensite, which are areas more reactive to corrosion [22,24].

3.4. Corrosion products analysis

Fig. 16 shows the SEM images of the sample surfaces after the polarization test, corresponding to 300Sol (Fig. 16(a)), 300E485 (Fig. 16 (b)), 300E560 (Fig. 16(c)), 350 Sol (Fig. 16(d)), 350E485 (Fig. 16(e)) and 350E560 (Fig. 16(f)). A surface covered with a thin layer of high degradation can be observed in all samples. It is also possible to observe pits and cracks in some areas of the material, suggesting dissolution. These cracks and pits have similarities with the degradation found by Masoumi et al. [18], Dai et al. [25] and Pawel et al. [26]. This degradation arises from the hydrogen reaction and inter-granular corrosion caused by the stress produced by the precipitation of intermetallic compounds in the grain boundaries and the preference of the HF to

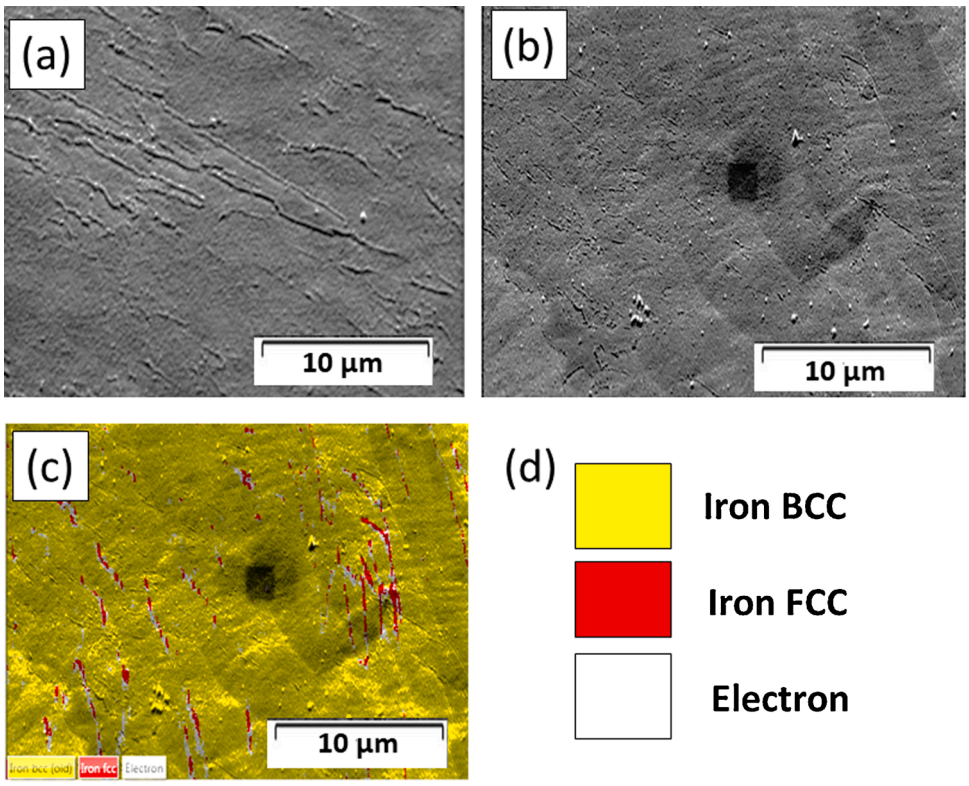

Fig. 10. SEM/EBSD image for the sample of grade 300 maraging steel aged at 560 °C for 3 h. In (a) the general region for the analyses, (b) selected region for the EBSD analyses, (c) EBSD map detecting the phases and (d) color legend for the phases.

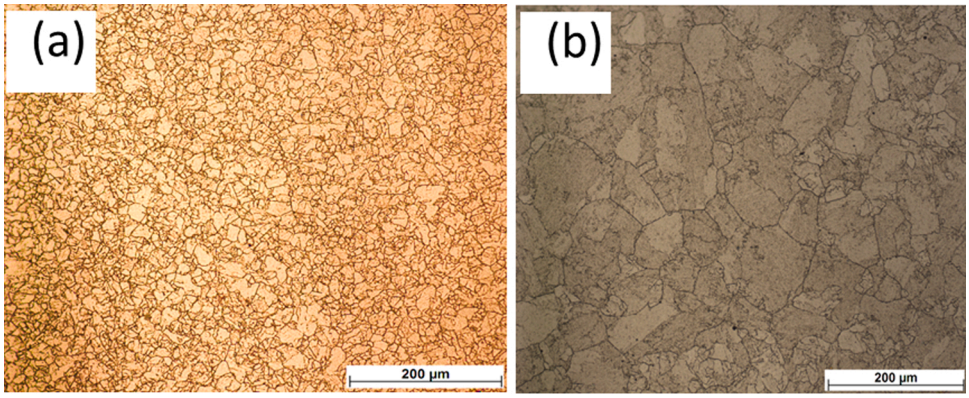

Fig. 11. Optical microscopy images of maraging steels (a) 300 and (b) 350 in the solution annealed at 840 °C for 1 h and aged at 560 °C for 3 h.

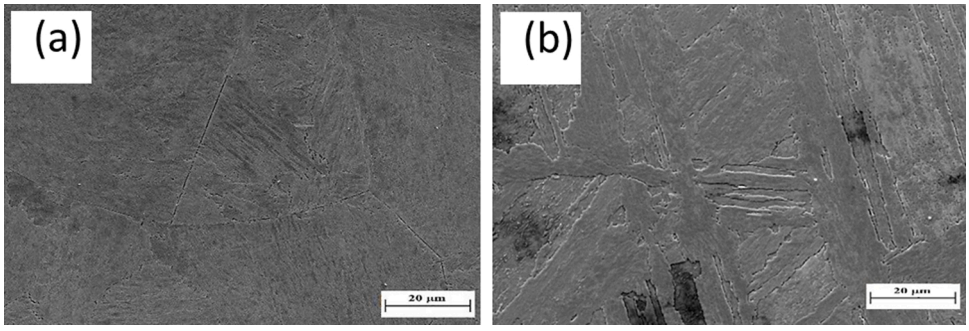

Fig. 12. SEM of the microstructure of maraging steels (a) 300 and (b) 350 solution annealed at 840 °C for 1 h and aged at 560 °C for 3 h.

Table 2
HRC hardness and prior autenite grain size of the grade 300 and 350 maraging steels in all the conditions studied.

Steel	Condition	Average hardness (HRc)	erro	Grain size (μm)
Mar 300	Sol. 840/1 h	34	0	24.6
Mar 350	Sol. 840/1 h	38	0	108.6
Mar 300	Sol. 840/1 h + env 480/ 3h	53.75	0.5	28.6
Mar 350	Sol. 840/1 h + env 480/ 3h	58.75	1	103.4
Mar 300	Sol. 840/1 h + env 560/ 1 h	50.75	1	28.1
Mar 350	Sol. 840/1 h + env 560/ 1 h	55.75	1.9	107.2

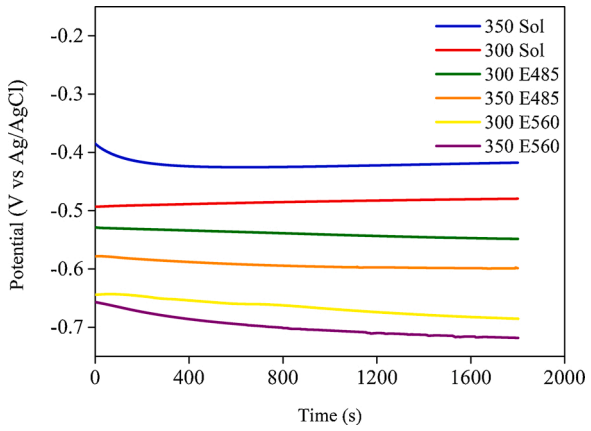

Fig. 13. OCP curves of the grade 300 and 350 Maraging steels in 0.01 M HF aqueous solution.

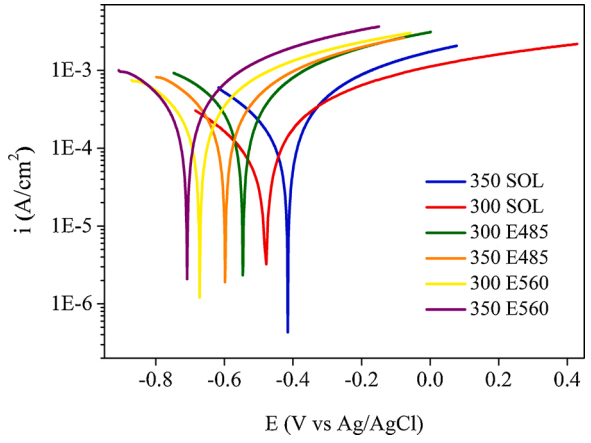

Fig. 14. Linear polarization curves of the grade 300 and 350 Maraging steels in 0.01 M HF aqueous solution.

dissolve these regions, as mentioned in the literature [10,18,24–31].

Linear EDS analysis was also performed on the surface of the steels. This result is shown in Fig. 17(a) and Table 4. The chemical composition detected in the most degraded areas showed fluorine and oxygen, together with the alloying elements of the steel. No morphological differences were found between the surfaces of grade 300 and grade 350 maraging steels under the conditions studied, but slight differences were found in the amount of elements in the corrosion product. With grade

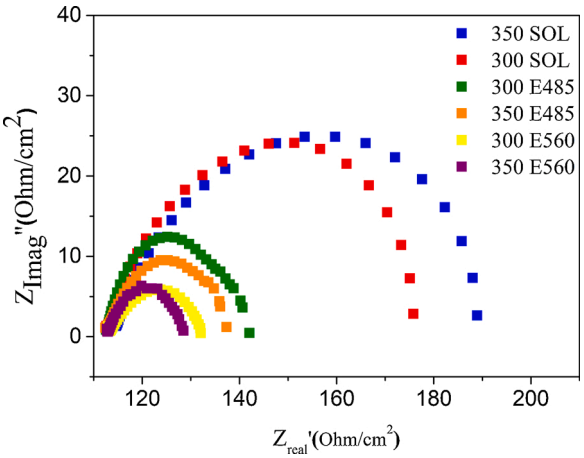

Fig. 15. EIS (Nyquist) curves of the grade 300 and 350 Maraging steels in 0.01 M HF aqueous solution.

Table 3
Electrochemical parameters taken from the electrochemical tests.

Sample	Z_{real} (Ohm/cm²)	OCP (V vs Ag/AgCl)	E_{corr} (V vs Ag/AgCl)	I_{corr} (A/cm²)
350 Sol	76	−0.42	−0.42	1.57×10^{-4}
300 Sol	63	−0.48	−0.48	1.28×10^{-4}
300 E485	29	−0.54	−0.54	1.97×10^{-4}
350 E485	24.5	−0.60	−0.60	1.70×10^{-4}
300 E560	19.3	−0.68	−0.68	1.70×10^{-4}
350 E560	15.5	−0.71	−0.71	2.30×10^{-4}

350 maraging steel, more cobalt and titanium were detected, which is the opposite result of grade 300 maraging steel. Fig. 17(b) shows that the areas most affected by degradation had increased percentage of fluoride in the chemical composition of the corrosion product. Table 4 shows the quantification of the chemical composition at points A (inside the dark crack) and B (degraded surface) on the degraded surface of grade 350 maraging steel in Fig. 17(a). The large molybdenum content found is attributed to the formation of oxide in this metal. According to Zhang et al. [27] this oxide has good stability in solutions with hydrofluoric acid, but the great affinity of iron, nickel, and cobalt to react with fluorine reduces the passive character of this oxide. Note that the oxygen and fluorine in the Tables of this study have only been taken into account for illustrative purposes.

Fig. 18 shows two Raman spectra of the steel surface after polarization tests, one for grade 300 and the other for grade 350 maraging steel. It is important to highlight that the study presented by Avelino [23] was used as a reference to show the possible corrosion products formed on the steel surface, considering that no references were found in studies related to corrosion resistance in maraging steel using HF solution. It was necessary to observe the few existing studies involving these steels with other acid solutions. The peaks found in samples of grade 300 maraging steel correspond to hematite Fe_2O_3 (293 cm^{-1}, 611 cm^{-1} and 1321 cm^{-1}) [32,33], FeF_2 (370 cm^{-1}, 500 cm^{-1} and 1080 cm^{-1}) [34], NiO (740 cm^{-1}, 910 cm^{-1} and 1040 cm^{-1}) [35], MoO_3 (667 cm^{-1}, 822 cm^{-1} and 1006 cm^{-1}) [36], and CoF_2 (787 cm^{-1}, 1118 cm^{-1} and 1214 cm^{-1}) [37]. In all conditions studied for grade 350 maraging steel, in addition to the previous compounds, TiO_2 peaks were also found (220 cm^{-1}, 440 cm^{-1} and 605 cm^{-1}) [38,39]. This can be attributed to the greater number of this element in this steel, which produces this oxide on the metal surface. The formation of all these corrosion products is the result of the HF dissociation process in H^+ and F- ions [40].

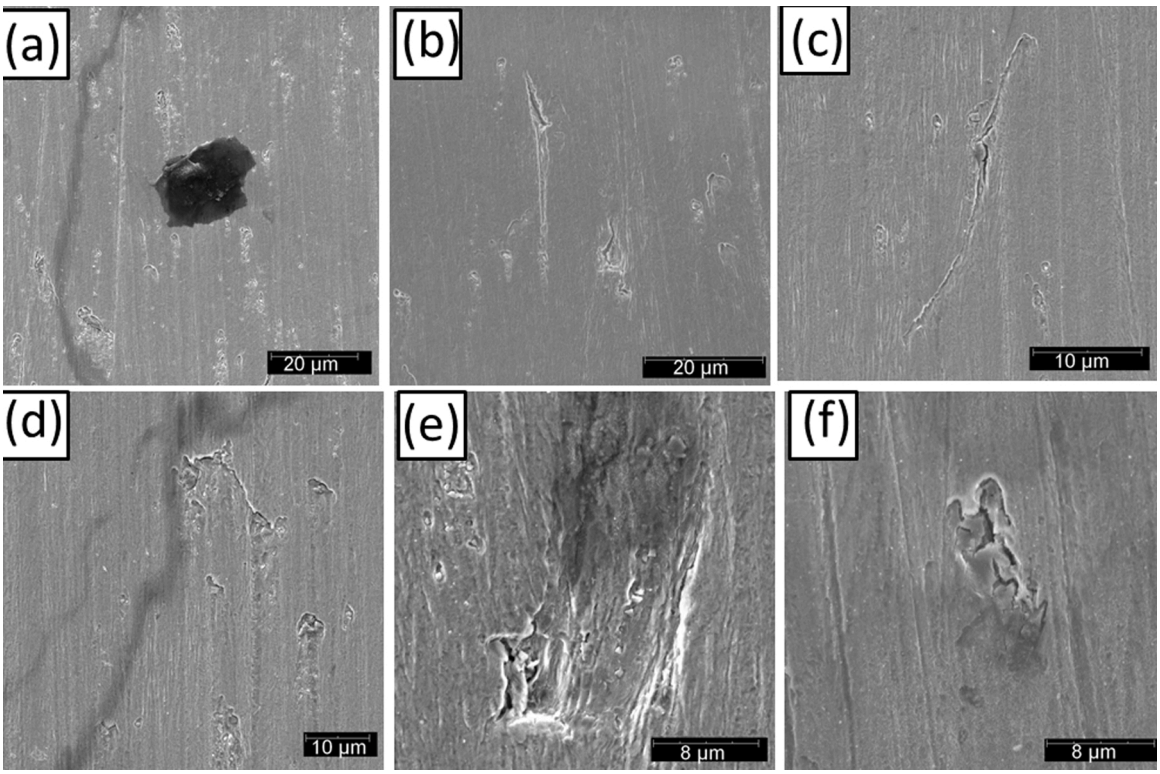

Fig. 16. SEM images of the surface degradation of 300 (a, b, c) and 350 (d, e, f) Maraging steels after polarization tests.

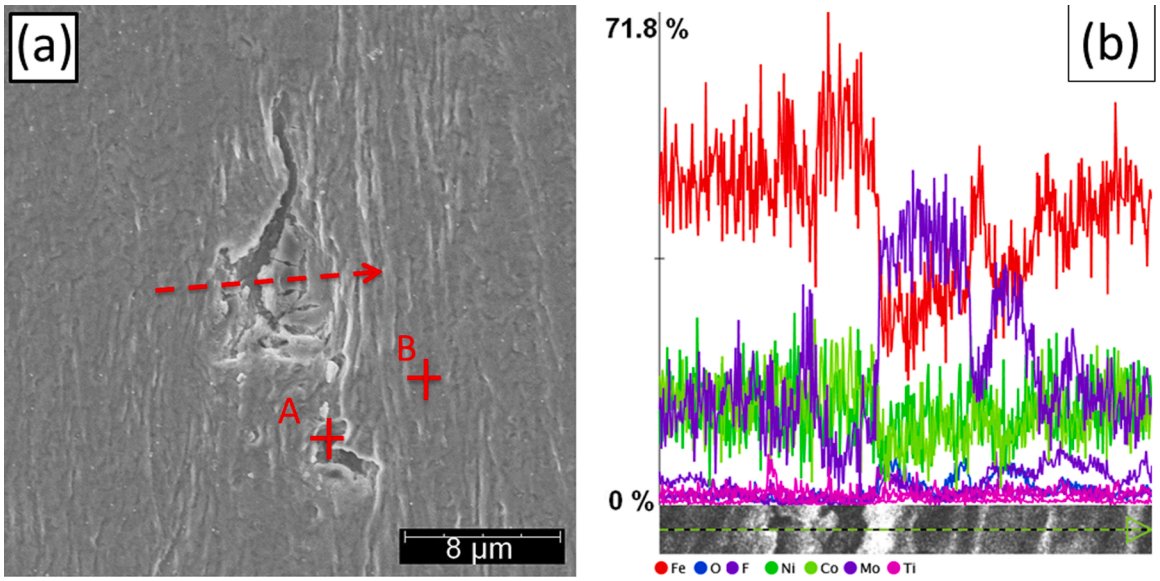

Fig. 17. a) SEM image and b) Linear EDS of the degraded surface of the grade 350 maraging steels.

Fluoride ion is highly reactive and reacts very easily with the alloying elements of the maraging steel, forming compounds of Metal-F_2 (MF_2) type [8,9,31], such as MoF_2, TiF_2, FeF_2, CoF_2, NiF_2.Soon after, depending on the HF concentration (low), some of these compounds react with water to form oxides according to the reaction in Eq. (1) [31].

$$MF_2 + H_2O \rightarrow MO + 2HF \quad (1)$$

Together with the previous reaction that provides oxygen, it is possible to form the MoO_3, Fe_2O_3, NiO, and TiO_2 oxides found on the steel surface. MoO_3 and TiO_2 oxides are known as protectors, but the low amount of these elements in steel is not sufficient to cover the entire surface [27], and the large amount of iron and nickel leads to the formation of much more Fe_2O_3 and NiO, which are not protective. It is important to observe the formation of HF that causes the continuous steel dissolution reaction. An important finding of Dai et al. [25] and Zhang et al. [27] shows that iron has a high affinity to the reaction with fluorine, and that the availability of this element increases the dissolution rate.

4. Conclusions

The results of the tests showed the effect of chemical composition

Table 4
Spot EDS measurements taken at the locations shown in the SEM image in Fig. 15a.

EDS quantitative analysis from A and B points (wt. %)			
Element Number	Element Symbol	Point A	Point B
26	Fe	48.34	49.43
8	O	4.75	6.84
9	F	15.02	9.69
27	Co	9.60	9.81
28	Ni	14.94	14.36
42	Mo	6.61	8.71
22	Ti	1.04	1.16

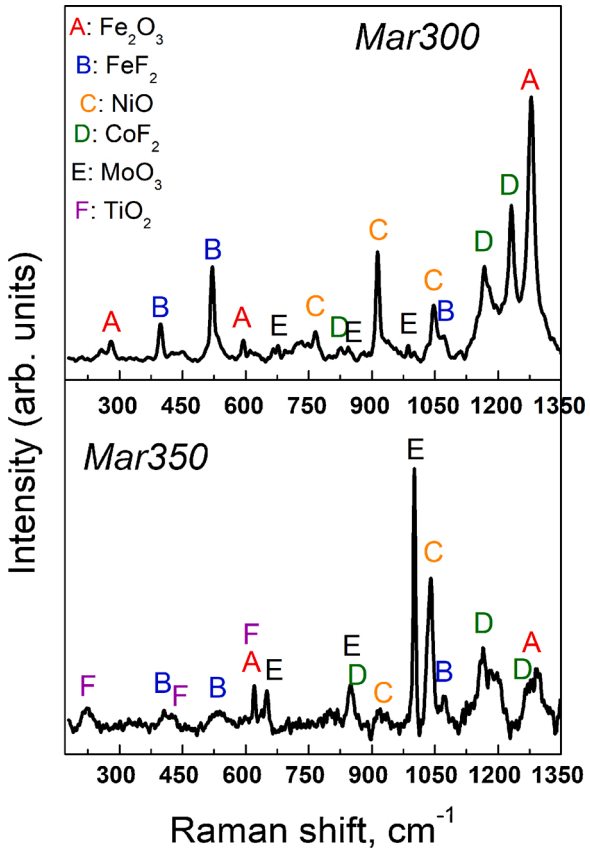

Fig. 18. Raman spectrum collected from the surface samples after polarization tests.

and heat treatments on the microstructure, mechanical properties, and corrosion resistance of grade 300 and grade 350 maraging steels.

The effect of the chemical composition led to some changes in the areas of phase stability shown in the thermodynamic diagrams. Although these results are similar in the two steel grades studied, some temperatures and quantities (mainly of intermetallic compounds) showed significant variations.

The maraging steels in the solution annealed condition showed a completely martensitic microstructure. Due to their size, it was not possible to detect and observe the intermetallic compounds precipitated in the aged conditions. The hardness values allowed to evaluate the influence of aging heat treatments on the well-known mechanical properties of these steels. Grade 300 maraging steel showed a higher hardness in all conditions, as expected. Both steels showed their lowest hardness values in the solution annealed condition. Among the aging conditions, it is possible to confirm that the aging condition at 480 °C for 3 h resulted in the highest hardness values because of the precipitation of nanometric intermetallic compounds. Lastly, the samples aged at 560 °C for 3 h showed a decrease in the hardness values precisely because of the reversion of austenite for both steels, which was detected by XRD and EBSD.

The electrochemical results showed that aging has a negative effect on the corrosion resistance of maraging steels. Solution annealed steels had a more noble behavior, and in this heat treatment condition, the higher amount of cobalt and titanium resulted in better corrosion resistance in grade 350 maraging steel compared to grade 300 maraging steel. The higher amount of intermetallic precipitates due to the increase of cobalt and titanium in grade 350 maraging steel decreased its corrosion resistance against grade 300 maraging steel in the aged conditions. This effect is caused by a larger area of phase contours and chemical composition differentials between the martensitic phase and these nanometric compounds that produce galvanic pair. In the aged conditions, it is possible to observe the effect that an additional phase (austenite) has in the decrease of the electrochemical behavior of the steels aged at 560 °C for 3 h. A greater area of grain boundaries and composition between phases increases the susceptibility of these steels.

The high reactivity of the fluoride ion (despite the low concentration of the solution) was decisive for the reaction with the alloy elements, mainly with iron and cobalt. Raman analysis results showed the formation of fluoride cobalt and iron compounds that are the primary effect of the steel dissolution. Some oxides that should protect the material, such as MoO_3 and TiO_2, were found. However, their effect is diminished by their low quantity and the high reactivity of fluorine in the dissolution of the other elements. The morphology of the steel surface after the polarization test was also observed, showing the deterioration of the steel with many cracks associated with the hydrogen susceptibility.

Declaration of Competing Interest

The authors declare that they have no known competing financial interests or personal relationships that could have appeared to influence the work reported in this paper.

Acknowledgments

The authors gratefully acknowledge the CAPES (Finance Code 001) and FUNCAP for providing the financial help and the CIEFMA Research Group-UPC and Multiscale Technology Research Center -UPC for providing the technical support.

References

[1] A. Magnee, J.M. Drapier, J. Dumont, D. Coutsourdis, L. Habraken, C.C.H.S. Steels, (1974) Centre D'Information Du Cobalt, Brussels.
[2] 18 Per Cent Nickel Maraging Steels: Engineering Properties, Nickel development institute, 1976. No. 4419.
[3] M. Schmidt, K. Rohrbach, Heat treating of maraging steels, in: ASM Int. ASM Handbook, 4, 1991, pp. 219–228.
[4] E.R. Petty, J. Appl. Cryst. 4 (1970) 402–403.
[5] H.J. Rack, D. Kalish, Metall. Mater. Trans. B 2 (1971) 2011–3020.
[6] U.K. Viswanathan, G.K. Dey, M.K. Asundi, Metall. Trans. A 24 (1993) 2429–2442.
[7] A. Glaser, Sci. Glob. Secur. 16 (2008) 1–25.
[8] S. Aftergood, C. Bidwell, M.A, Fisher, M. Korda, H. Kristensen, A. Mount, M. Trent, Engineering Considerations for Gas Centrifuges.
[9] D.B. Bradhurst, P.M. Heuer, Corrosion 37 (1981) 63–70.
[10] T. Poormina, J. Nayak, A.N. Shetty, Int. J. Electrochem. Sci. 5 (2010) 56–71.
[11] B.S. Sanatkumar, J. Nayak, A.N. Shetty, Chem. Eng. Commun. 199 (2012) 1610–1625.
[12] P. Kumar, A.N. Shetty, Port. Electrochim. Acta 31 (2013) 21–32.
[13] J.M. Pardal, S.S.M. Tavares, M.P. Cindra Fonseca, H.F.G. Abreu, J.J.M. Silva, J. Mater. Sci. 41 (2006) 2301–2307.
[14] L.P.M. Santos, M. Bêres, I.N. Bastos, S.S.M. Tavares, H.F.G. Abreu, M.J.G. Silva, Corros. Sci. 101 (2015) (2015) 12–18.
[15] M.J.G. Silva, J.L. Cardoso, D.S. Carvalho, L.P.M. Santos, L.F.G. Herculano, H.F. G. Abreu, J.M. Pardal, Int. J. Hydrogen Energy 44 (2019) 18606–18615.
[16] American Society for Testing and Materials (Filadelfia, Pennsylvania), ASTM E112-96 (2004) e2: Standard Test Methods for Determining Average Grain Size, ASTM, 2004.
[17] V. Lima Filho, I. Barrosa, H.F. Gomes De Abreu, Mater Res. 20 (2017) 10–14.

[18] M. Masoumi, H.F.G. Abreu, L.F.G. Herculano, J.M. Pardal, S.S.M. Tavares, M.J. G. Silva, Eng. Fail. Anal. 104 (2019) 379–387.
[19] F.F. Conde, J.D. Escobar, J.P. Oliveira, M. Béreš, A.L. Jardini, W.W. Bose, J. A. Avila, Mater. Sci. Eng. A 758 (2019) 192–201.
[20] L.P.M. Santos, M. Beres, M.O. de Castro, P.W.C. Sarvezuk, L. Wu, L.F.G. Herculano, A. Paesano Jr, C.C. Silva, M. Masoumi, H.F.G. de Abreu, JOM 72 (2020) 3502–3512.
[21] U.K. Viswanathan, G.K. Dey, V. Sethumadhavan, Mater. Sci. Eng. A 398 (2005) 367–372.
[22] G.A. El-Mahdy, M.M. Hegazy, F.-E.L.-Taib Heakal, H.E. Mahmoud, A.M. Fathy, F. M. Sayed, Int. J. Electrochem. Sci. 8 (2013) 2816–2825.
[23] A.F. Avelino, W.S. Araújo, D.F. Dias, L.P. DOS Santos, A.N. Correia, P. Lima-Neto, Electrochim. Acta 286 (2018) 339–349.
[24] R.G. Madhusudhan, R.K. Srinivasa, Def Technol. 11 (2015) 48–55.
[25] H. Dai, S. Shi, C. Guo, X. Chen, Corros. Sci. 166 (2020), 108443.
[26] S.J. Pawel, Corrosion 50 (1994) 963–971.
[27] C. Zhang, Y. Li, Y. Hou, N. Tang, K. Ohmura, Y. Koizumi, A. Chiba, Corros. Sci. 89 (2014) 81–92.
[28] J. Rezek, I.E. Klein, J. Yhalom, Corros. Sci. 39 (1997) 385–397.
[29] G. Bellanger, J.J. Romeau, J. Nucl. Mater. 228 (1996) 24–37.
[30] T. Poormina, J. Nayak, A.N. Shetty, Corros. Sci. 53 (2011) 3688–3696.
[31] J.R. Crum, G.D. Smith, M.J. McNallan, S. Hirnyj, in: Presented at Corrosion'99 Nace International Conference, San Antonio, USA, 25-30 April, 1999, p. 382.
[32] D.L.A. De Faria, F.N. Lopes, Vib. Spectrosc. 45 (2007) 117–121.
[33] R. Guo, L. Dang, Z. Liu, Z. Lei, Colloid Surf. A 602 (2020), 125110.
[34] S.R. Chinn, H.J. Zeiger, in: Presented at American Institute of Physics: Conference Proceedings 5, Chicago, USA, 1971, p. 344.
[35] N. Mironova-Ulmane, A. Kuzmin, I. Steins, J. Grabis, I. Sildos, M. Pärs, Presented at Journal of Physics: Conference Series'93 Riga, Latvia, 2-4 April, 2007, 012039.
[36] N. Zhao, H. Fan, M. Zhang, J. Ma, Z. Du, B. Yan, H. Li, X. Jiang, Chem. Eng. J. 390 (2020), 124477.
[37] J.T. Hoff, P.A. Grungerg, J.A. Koningstein, Appl. Phys. Lett. 20 (1972) 358.
[38] T. Mazza, E. Barborini, P. Piseri, P. Milani, D. Cattaneo, A. Li Bassi, C.E. Bottani, C. Ducati, Phys. Rev. B 75 (2007), 045416.
[39] S.A. Abdullah, M.Z. Sahdan, N. Nayan, Z. Embong, C.R. Che Hak, F. Adriyanto, Mater. Lett. 263 (2020), 127143.
[40] L. Yu, Y. Jiang, Y. He, C.T. Liu, J. Alloys Compd. 638 (2015) 7–13.